Journal of Natural Gas Science and Engineering 94 (2021) 104110

Contents lists available at ScienceDirect

Journal of Natural Gas Science and Engineering

journal homepage: www.elsevier.com/locate/jngse

Factors influencing the in-situ stress orientations in shales: A case study of the Wufeng-Longmaxi formations in the Jiaoshiba Area, southeastern Sichuan Basin, China

He Tian [a,b], Lianbo Zeng [a,b,*], Xiang Xu [a,b], Hong Li [a,c], Bing Luo [d], Shaoqun Dong [a,e]

[a] State Key Laboratory of Petroleum Resources and Prospecting, China Petroleum University (Beijing), Beijing, 102249, China
[b] College of Geosciences, China University of Petroleum (Beijing), Beijing, 102249, China
[c] College of Petroleum Engineering, China University of Petroleum (Beijing), Beijing, 102249, China
[d] Research Institute of Petroleum Exploration and Development, SINOPEC Jianghan Oilfield Company, Wuhan, Hubei, 430223, China
[e] College of Science, China University of Petroleum, Beijing, 102249, China

ARTICLE INFO

Keywords:
Shale
Wufeng-longmaxi formation
Sichuan basin
In-situ stress orientation
Influence factor

ABSTRACT

Determining the present-day stress orientation is essential for the exploration and development of shale gas. The Longmaxi Formation is the most significant shale gas reservoir in the Jiaoshiba Area of the Sichuan Basin, China. However, little is known about the orientation of the maximum horizontal stress (S_{Hmax}) and the factors influencing it within the formation. In this study, the orientation of the S_{Hmax} in the Jiaoshiba Area was determined based on observations of drilling-induced fractures on resistivity image logs. Then, the tectonic activity, the mechanical properties of the rock, and finite element simulations were studied in detail to determine the major factors influencing the S_{Hmax} orientation in the Jiaoshiba Area. The results show that the S_{Hmax} orientation within the study area ranges from nearly EW to NEE-SWW. The vertical variations of the in-situ stress orientation are controlled by the structural strength and the mechanical properties of the rock. In the area that has experienced intense tectonic movements, the deviation in the S_{Hmax} orientation (from 30° to 80°) was caused by the differences in the mechanical properties of the rocks. The finite element simulations indicate that the lateral variations in the S_{Hmax} orientation was mainly controlled by the faults. The stress rotation near the end of the fault is 14°–21° higher than that in the middle of the fault. Furthermore, the stress variation caused by the mechanical properties of the fault zone ranges from 12° to 18°, and this deviation increases as the Young's modulus of the fault zone decreases. In the study area, the azimuth deflection (18°–46°) of the S_{Hmax} orientation influenced by the NE faults is higher than that (12°–36°) influenced by the nearly NS faults, which is the main reason for the lateral stress rotation.

1. Introduction

Shale reservoirs are characterized by low porosity, low permeability and strong heterogeneity, producing hydrocarbons from tight shale reservoirs depends on successful hydraulic fracturing (Huggins et al., 2008; Gale et al., 2007). The present-day in-situ stress field is a significant geological parameter influencing successful hydraulic fracturing operations within shale reservoirs. The orientation of the present-day maximum horizontal stress affects the direction of hydraulic fracture (Nasehi and Mortazavi, 2013; Ameen, 2014; Zangeneh et al., 2014; Karatela et al., 2016; Mohammadnejad and Andrade, 2016), and controls the aperture, permeability and opening pressure of natural fractures in the low permeability shale reservoirs (Finkbeiner et al., 1997; Zeng and Li, 2009; Bisdom et al., 2016). Furthermore, it can comprehensively influence on hydrocarbon migration and accumulation underground, reservoir management, borehole stability and fault reactivation (Barton et al., 1995; Sibson, 1996; Jones and Hillis, 2003; Goodman and Connolly, 2007; Tingay et al., 2010a; Rajabi et al., 2016). Therefore, knowledge of the present-day S_{Hmax} orientation is an indispensable issue in unconventional hydrocarbon exploration and development.

Recently, many researchers have highlighted the significance of smaller basin and field scale perturbations in the stress field. Knowledge of the variation of S_{Hmax} orientation at these scales contributes to a

* Corresponding author. State Key Laboratory of Petroleum Resources and Prospecting, China Petroleum University (Beijing), Beijing, 102249, China.
E-mail address: lbzeng@sina.com (L. Zeng).

https://doi.org/10.1016/j.jngse.2021.104110
Received 22 June 2020; Received in revised form 13 April 2021; Accepted 19 June 2021
Available online 24 June 2021

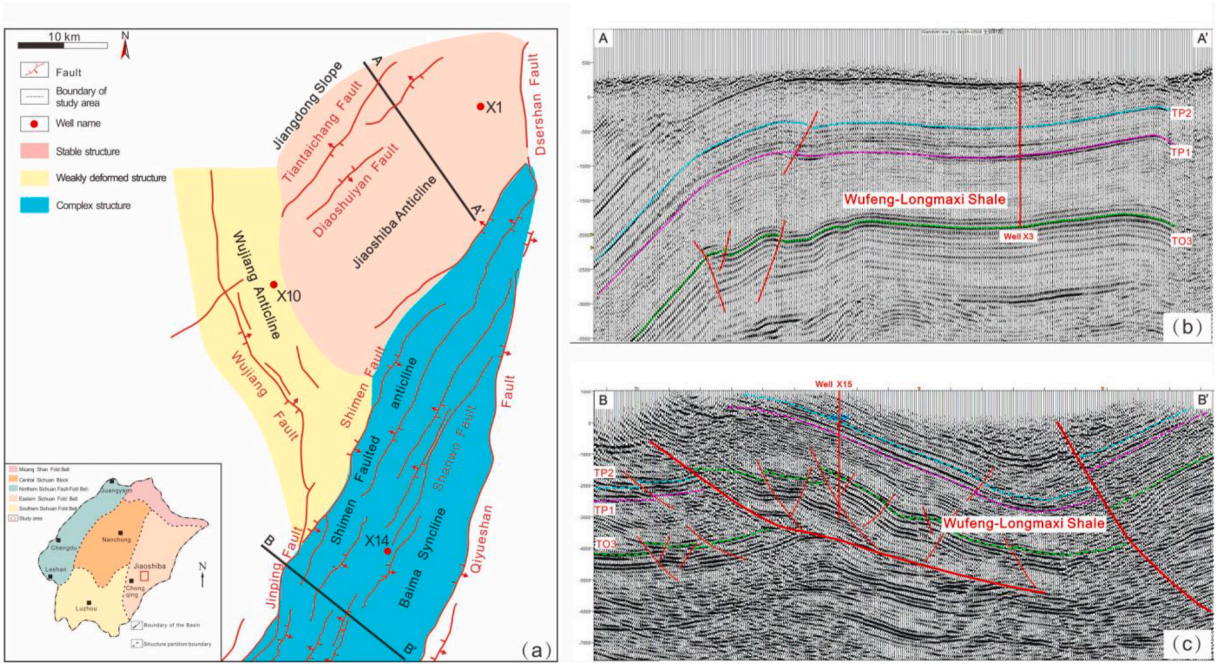

Fig. 1. (a) Schematic location and tectonic unit of the Jiaoshiba Area. (b) The seismic section A-A′ in stable area. (c) The seismic section B–B′ in complex area.

better understanding of the petroleum applications. Previous studies have reported that different local structural patterns, variable mineral compositions, rock mechanical properties, faults are the main geological factors affecting the S_{Hmax} orientation in many sedimentary basins worldwide (Bell, 1996a, 1996b, 1996b; Cuss et al., 2003; Shen et al., 2007; Brooke-Barnett et al., 2015; Alt and Zoback, 2016; Rajabi et al., 2017).

Wufeng-Longmaxi shale is widely distributed with great thickness, high quartz content, high organic matter content and gas content, which is the major target for shale gas exploration and development in Jiaoshiba Area, Southeastern Sichuan Basin. At present, Jiaoshiba Area has become the largest commercial shale-gas field in China. The study area has been mainly affected by the strong compression of the Yanshanian-Himalayan movement since the Indosinian period, and has undergone various transformations such as structural deformation, uplift and denudation, and fluid flow, which caused the tectonic stress field varies greatly in different periods, regions, structural positions and depths (He et al., 2018). In recent years, geologists have carried out some studies on the magnitude of the in-situ stress in the study area (Tian et al., 2019). However, little is known about the distribution and influence factors of the present-day in-situ stress orientations, which limits the development of shale gas in the Jiaoshiba Area. To address this gap in the research, drilling induced fractures were interpreted from 15 resistivity image logs to determine the distribution and variation of maximum horizontal stress orientation both in depth and laterally. Then, the structural deformation intensity of different areas, mechanical properties of different layers were determined and 17 simplified geological models of fault were established to assess the influence factors of S_{Hmax} orientation. The results could provide a geological reference for hydraulic fracturing in Jiaoshiba Area of the Southeastern Sichuan Basin, China.

2. Geological settings

The Jiaoshiba Area is situated in the Fuling District of Chongqing municipality, China. Tectonically, the Jiaoshiba Area is part of the Southeastern Sichuan Basin, which experienced multiple tectonic movements since the formation of Yangtze Para platform (Ma et al., 2016; Guo et al., 2013). The Jiaoshiba Area is controlled by two groups of faults trending in a North-East direction (Daershan fault, Shimen-Jinping fault, Diaoshuiyan fault, Tiantaichang fault et al.) and a nearly north-south direction (Wujiang Fault) (Fig. 1a) (Guo and Zhang, 2014; Tian et al., 2020). Taking Shimen fault as the boundary, the Jiaoshiba Area can be divided into north and south area. The north area can be subdivided into Jiaoshiba anticline, Jiangdong slope and Wujiang faulted anticline. The south area can be subdivided into Shimen faulted anticline and Baima syncline. The main body of the Jiaoshiba anticline has little deformation and is characterized by a box-shaped anticline with gentle stratum and undeveloped faults (Fig. 1b) (Hu et al., 2014; She et al., 2016; Xu et al., 2021). However, the Shimen faulted anticline has strong deformation, developed faults and large dip angles (Fig. 1c). Based on the comprehensive analysis of tectonic stress, structural form and fracture development degree (Table 1), the structural type in the Jiaoshiba Area can be divided into three types: stable type,

Table 1
Classification criteria of Structural types (adapted from Shu et al., 2018).

Structural type	Structural form	Deformation strength	Fault	Fracture	Typical well
Stable type	Gentle anticline、Slope, gentle syncline	The stratum is gentle. The formation thickening is not obvious.	Faults are not developed. Faults displacement is less than 100 m.	Fractures are not developed	X1
Weakly deformed type	Faulted anticline, faulted nose structure	The stratum dip angle is larger than 10°. The thickening ratio of formation is less than 1.5.	Faults are developed. Faults displacement is 100–500 m.	More than 10 fractures are developed per 100 m	X10
Complex type	Narrow faulted-anticline, complex fault zone	The stratum dip angle is 10°–35°. The thickening ratio of formation is about 2.	Faults are developed. Faults displacement is larger than 500 m.	Dozens of fractures are developed per 100 m	X14

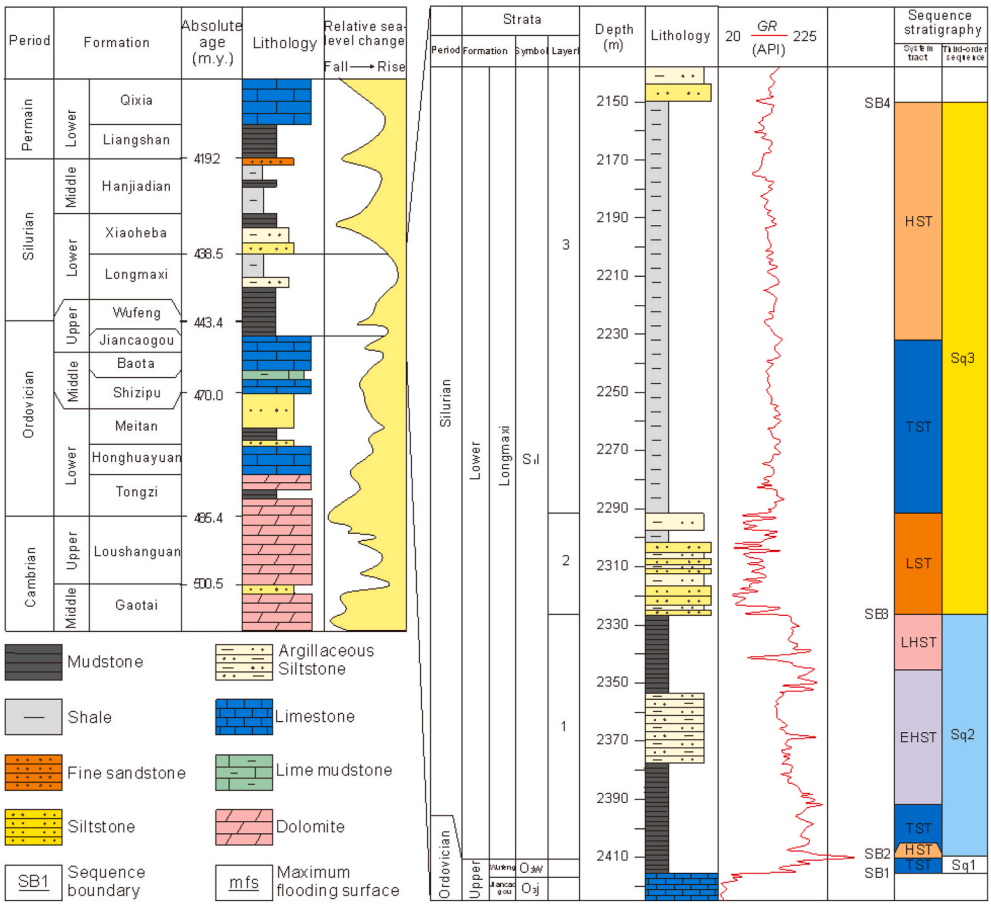

Fig. 2. Generalized stratigraphic diagram of the Jiaoshiba Area, Southeastern Sichuan Basin (adapted from Guo et al., 2017).

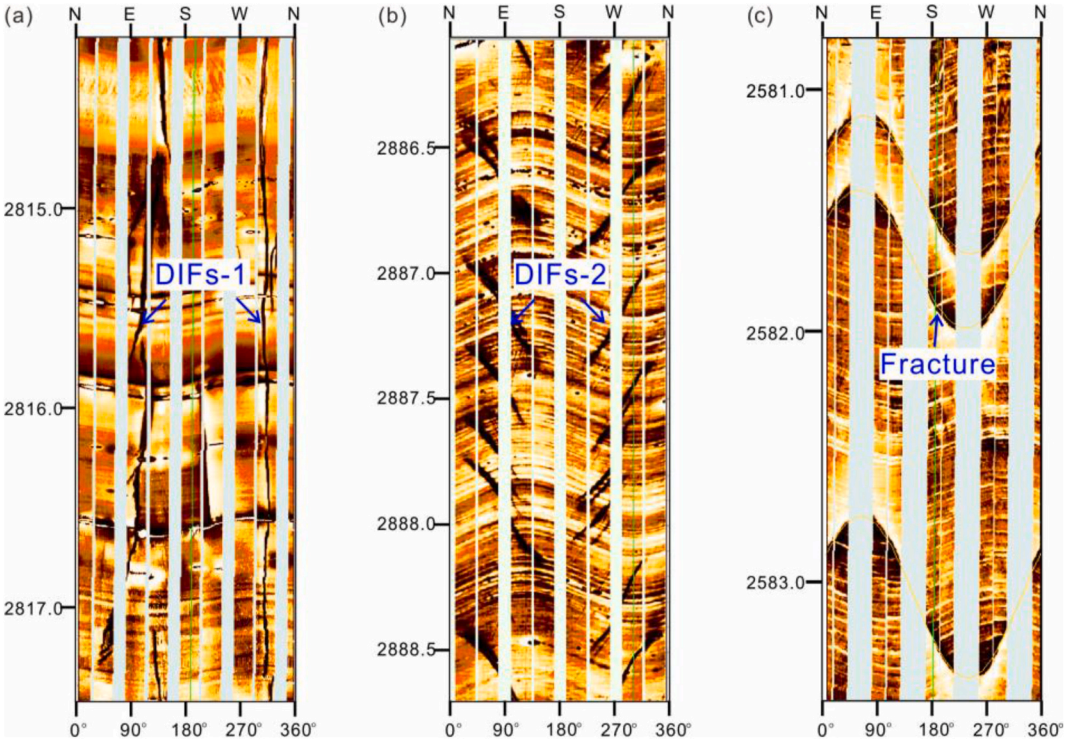

Fig. 3. DIFs and natural fractures interpreted from borehole imaging logs in the Jiaoshiba Area. (a) The first type of DIF (DIFs-1). (b) The second type of DIF (DIFs-2). (c) Natural fractures.

weakly-deformed type and complex type (Fig. 1a) (Shu et al., 2018).

The shale in the Jiaoshiba Area is mainly developed in the Upper Ordovician Wufeng Formation (O_3w) and the Lower Silurian Longmaxi Formation (S_1l), of which overlying strata is the Lower Silurian Xiaoheba Formation, and the underlying strata is grey nodular limestone of the Upper Ordovician Jiancaogou Formation and the Middle Ordovician Baota Formation (Fig. 2). The Longmaxi Formation can be divided into three members: Long 1(S_1l^1), Long 2(S_1l^2), and Long 3 (S_1l^3) (Fig. 2). The lithology of the Long 1 Member is dominated by black shale rich in organic matter, high maturity and brittleness. The Long 2 Member is characterized by siltstone with argillaceous siltstone, and the lithology of Long 3 Member is mainly light grey mudstone (Guo et al., 2017). Drilling results show that the thickness of the O_3w-S_1l shale in the Jiaoshiba Area is about 50 m–600 m, with the high gas-bearing shale at approximately 38 m–42 m (Hu et al., 2014; Gao et al., 2017; Yi, 2017). As the primary stratum for commercial shale gas production in the Jiaoshiba Area, the mineralogical components of the Wufeng-Long 1 Member contains lots of brittle minerals, including quartz and feldspar, and lower content of clay and carbonate minerals. The total organic carbon (TOC) ranges from 2.0% to 6.5% and vitrinite reflectance (Ro) ranges from 2.0% to 3.6% (Guo et al., 2014; Wei et al., 2016; Wu et al., 2019). The average porosity and permeability of the Wufeng-Long 1 Member shale is 4.87% and 21.5mD, respectively (Guo et al., 2016; Shu et al., 2018). The pressure coefficient of the Wufeng-Long 1 Member shale ranges from 1.3 to 1.5, indicating that the Jiaoshiba Area is in overpressure state, which is conducive to shale gas preservation (Guo et al., 2017).

3. Methods and materials

3.1. Drilling induced fractures from borehole imaging logs

The orientation of the present-day S_{Hmax} is an essential component of the stress tensor which has obtained extensive attention since the exploration and development of unconventional resources in recent years. (Bell, 1996b; Tingay et al., 2005b; Zoback, 2007; Barton and Moos, 2010). Interpretation of drilling induced fractures from borehole imaging logs are considered as the most common way to obtain the orientation of the S_{Hmax} (Bell and Gough, 1979; Bell, 1996a; Zoback, 2007). Drilling induced fractures (DIFs) form when the minimum circumferential stress becomes tensile and exceeds the tensile strength of borehole wall. Such DIFs are parallel to the orientation of the S_{Hmax} in vertical wells. (Pes̈ka & Zoback, 1995; Brudy and Zoback, 1999; King et al., 2008). Based on the observation of borehole imaging logs, DIFs can be divided into two manners. One is DIFs-1, which appear on resistivity image logs as pairs of vertically or near-vertically dark fractures parallel to the borehole axis and are always separated by 180°(Fig. 3a) (Aadnoy and Bell, 1998; Brudy and Zoback, 1999; Zoback et al., 2003). Another is DIFs-2, which are shown on resistivity image logs as two groups of echelon fractures separated by 180° and inclined relative to the borehole axis (Fig. 3b). DIFs-2 are distinguished from pre-existing natural fractures on resistivity image logs by their discontinuous nature; whereas natural fractures usually occur as continuous sinusoids (Fig. 3c) (Barton and Zoback, 2002; Barton et al., 2009; Ju et al., 2018).

3.2. Finite element simulation

Finite element simulation is an important method for quantitative analysis of in-situ stress (Kaiser et al., 2005; Barba et al., 2010; Zeng et al., 2019). The influence of different geological factors on the orientation of the S_{Hmax} in shale could be analyzed by finite element (FE) numerical simulation.

3.2.1. FE technique

Geological bodies are considered as the finite continuous elements connected by nodes in FE technique. Each element is assigned appropriate mechanical parameters based on the rock mechanics experiment. Then, the interaction of stress, strain and displacement of each node is analyzed and calculated under the external regional tectonic stress, so as to reflect the variation of stress field of the geological body (Ding et al., 2012; Zeng et al., 2013; Ju et al., 2018).

The displacement u and v of any point (x, y) in the element can be expressed in the following form Eq. (1):

$$\begin{cases} u = u(x, y) \\ v = v(x, y) \end{cases} \tag{1}$$

where u, v are displacements along the x, y axes.

Bases on geometric equation, strain and displacement exhibit the following relationship:

$$\begin{cases} \varepsilon_x = \dfrac{\partial u}{\partial x} \\ \varepsilon_y = \dfrac{\partial v}{\partial y} \\ \varepsilon_{xy} = \dfrac{\partial u}{\partial y} + \dfrac{\partial v}{\partial x} \end{cases} \tag{2}$$

The strain matrix can be expressed as follows Eq. (3).:

$$[\varepsilon] = [B][\delta]^e \tag{3}$$

where $[B]$ is the geometric matrix, $[\delta]$ is the nodal displacement matrix.

According to the principle of virtual displacement, the integral nodal load matrix can be derived as follows (Eq. (4))

$$[P] = [K][\delta] \tag{4}$$

where $[P]$ is the integral nodal load matrix, $[K]$ is the integral stiffness matrix, $[\delta]$ is the nodal displacement matrix for the integral structure of the examined elemental array.

Based on the elastic mechanics equation, the relationship between stress and strain follows Eq. (5).

$$[\sigma] = [D][\varepsilon] \tag{5}$$

where $[D]$ is the elasticity matrix.

3.2.2. Geological model setup

In this study, 17 simplified geological models of fault were established to assess the influence of fault on S_{Hmax} orientation under the same boundary conditions. Firstly, keeping the angle between fault and regional stress constant, effects of mechanical properties of the fault zone on stress orientation were analyzed by reducing the mechanical properties of the fault zone. Then, increasing the angle between fault and regional stress orientation to analyze the angle between fault and regional stress orientation on stress deviation. Accurate mechanical properties of the fault zone are difficult to obtain. According to the previous studies, faults were usually defined as “weak zones”, where young’s modulus is usually lower than that of the surrounding rocks, while Poisson’s ratio is usually larger than that of the surrounding rocks (Jiu et al., 2013; Ju and Sun, 2016; Ju et al., 2017). In the initial fault zone, the young’s modulus E_1 is 7 GPa, and the Poisson’s ratio μ_1 is 0.25. In this study, the rock mechanical parameters of shale were obtained by triaxial compression test with MTS815 flex test GT. under 20 MPa confining pressure. The young’s modulus E_2 = 35 GPa and Poisson’s ratio μ_2 = 0.2 were used in geological models.

3.2.3. Boundary conditions

Due to little prior information on the S_{Hmax} orientation could be obtained from the world stress Map Database (Heidbach et al., 2016a, b) and lacking of earthquake focal mechanism solutions in the study area. The orientation of the regional stress was mainly determined based on the analysis of regional tectonic movement and resistivity image logs,

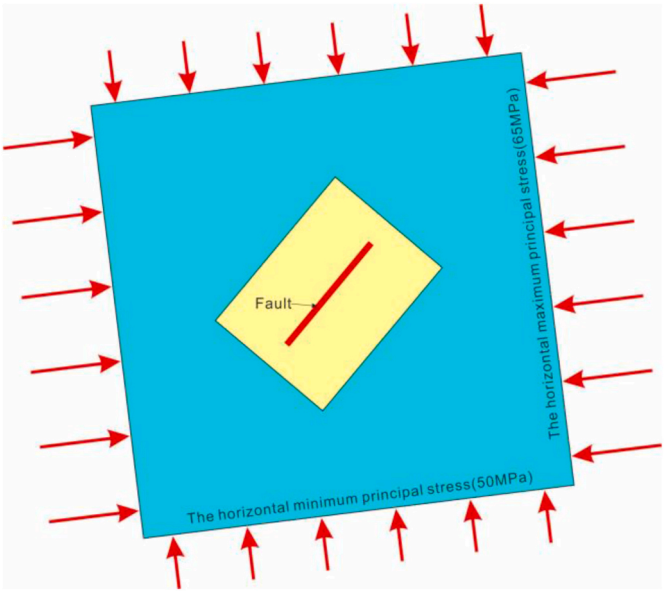

Fig. 4. Simplified nested model and stress loading scheme of the finite element simulation in the Jiaoshiba area.

which is nearly EW-trending (83°) (Hu et al., 2010). The boundary stress magnitude was determined based on the interpretation of dipole acoustic logs. The boundary maximum horizontal stress (σ_H) is 65 MPa, and the minimum horizontal stress (σ_h) is 50 MPa. Meanwhile, the initial fault model was nested within a larger square to facilitate applying forces and eliminate the boundary effects (Fig. 4.)

4. Results

In this study, approximately 5.0 km of resistivity borehole imaging logs from 15 wells were interpreted to determine the DIFs in the Jiaoshiba Area. Drilling induced fractures were observed in 8 wells in the Jiancaogou Formation, 13 wells in the Wufeng-Long 1 Member, and 15 wells in the Long 2, 3 Members. The results show that the vertical variation in the maximum horizontal stress orientation between the Wufeng-Long 1 Member and the Long 2,3 Members ranges from 0° to 40°, and most are less than 10° (Fig. 5a, Table 2). Only in well X11 is the maximum deviation 40° (Fig. 5b). The azimuth deviation of the maximum horizontal stress is 0°–30° between the Wufeng-Long 1 Member and the Jiancaogou Formation in the Jiaoshiba anticline and the Jiangdong slope. The azimuth deviation of the S_{Hmax} orientation in the Wujiang faulted anticline and the Shimen anticline is 30°–80° (e.g., X13, X14, X15) (Fig. 5c and d; Table 2). Laterally, the orientation of the S_{Hmax} in the Jiaoshiba anticline and the Jiangdong Slope is nearly EW; while in the Wujiang faulted anticline and the Shimen faulted anticline, it is NEE. Specially, the S_{Hmax} orientation in X15 well is NNW (Fig. 6).

In order to compare the differences of the mechanical properties between the target formation and it's upper and lower adjacent formation, the mechanical parameters of the rocks were calculated from data of the dipole acoustic logs and density in 9 wells. The Young's modulus and Poisson's ratio of shale in the Wufeng–Long 1 Member is 38 GPa–43.8 GPa and 0.213–0.253, respectively. The Young's modulus and Poisson's ratio of shale in the Long 2, 3 Members is 38 GPa–43.8 GPa and 0.252–0.278, respectively. The Young's modulus and Poisson's ratio of limestone in the Jiancaogou Formation is 69 GPa–73GPa and 0.3–0.322, respectively (Fig. 7).

5. Discussion

5.1. Effects of the mechanical properties of the rocks on the orientation of S_{Hmax}

Variations in the S_{Hmax} orientation with burial depth have been observed in many sedimentary basins worldwide. This may result from the local structural patterns, mineral compositions, mechanical properties, faults, natural fractures, and/or bedding planes (Bell, 1996a, 1996b, 1996b; Cuss et al., 2003; Brooke-Barnett et al., 2015; Rajabi et al., 2017; Ju et al., 2018; Zeng et al., 2019). In the Jiaoshiba area, the vertical variations in the S_{Hmax} orientation wareere mainly influenced by the structural strength and the mechanical properties of the rocks, especially elasticity modulus. The Young's modulus of the shale in the Long 2, 3 Members is slightly higher than that of the shale in the Wufeng-Long 1 Member. The deviation in the S_{Hmax} orientation resulting from the difference in the mechanical properties between the two formations is usually less than 10°. However, the maximum vertical variation in well X11 is 40°. A detailed analysis of the imaging logs revealed that there are 38 micro-faults in well X11. These micro-faults

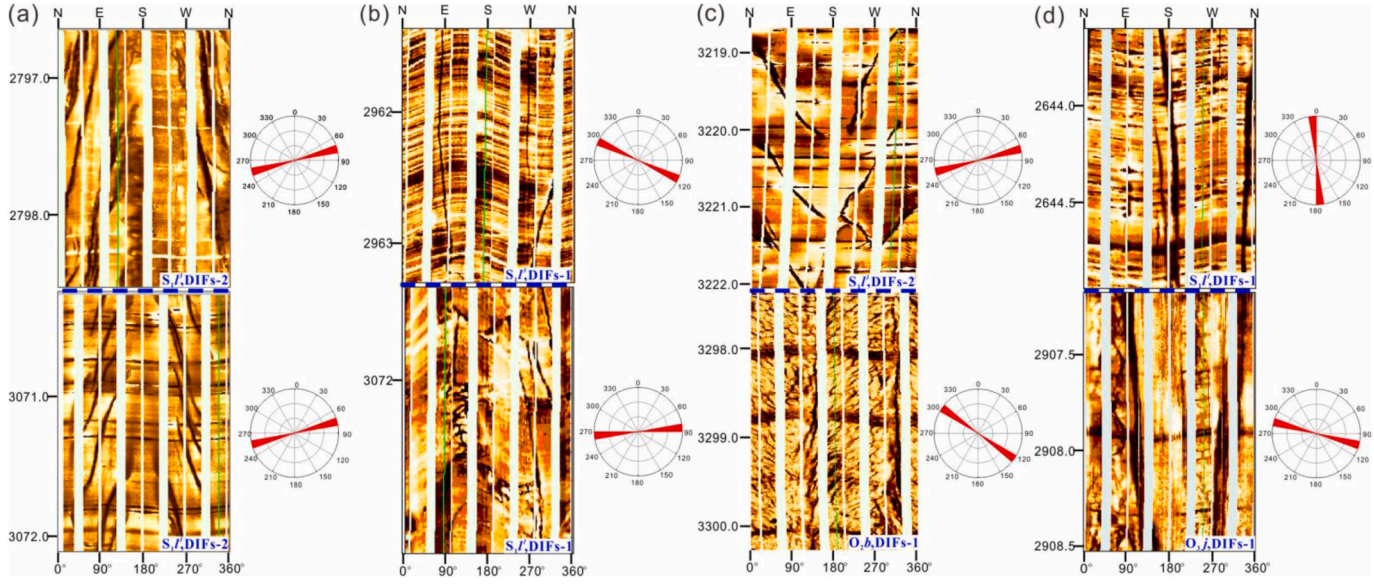

Fig. 5. Typical examples showing DIFs rotations observed in borehole imaging logs in the Jiaoshiba Area. Rose diagrams illustrate the present-day S_{Hmax} orientation. (a) Well X12 (b) Well X11 (c) Well X14 (d) Well X15 (See Fig. 6 for the well name).

Table 2
S_{Hmax} orientations derived from drilling induced fractures analysis in different stratigraphic regions.

Well	Average S_{Hmax} azimuth of O_2b-O_3j (°N)	Deviation of stress direction (°)	Average S_{Hmax} azimuth of O_3w-S_1l^1 (°N)	Deviation of stress direction (°)	Average S_{Hmax} azimuth of S_1l^2-S_1l^3 (°N)	Deviation of stress direction (°)	Deviation of S_{Hmax} azimuth between O_2b-O_3j and O_3w-S_1l^1, *aver(min-max)* (°)	Deviation of S_{Hmax} azimuth between O_3w-S_1l^1 *and* S_1l^2-S_1l^3, *aver (min-max)* (°)
1	–	–	88	±5	90	±10	–	2/(0–20)
2	–	–	88	±5	90	±10	–	2/(0–20)
3	–	–	71	±5	75	±5	–	4/(0–10)
4	65	±5	73	±5	75	±10	8/(0–20)	2/(0–20)
5	105	±10	93	±15	95	±15	12/(0–20)	2/(0–20)
6	–	–	92	±5	95	±10	–	3/(0–10)
7	90	±10	85	±10	90	±20	5/(0–30)	5/(0–30)
8	–	–	75	±5	85	±10	–	10/(0–10)
9	–	–	–	–	80	±5	–	–
10	–	–	–	–	85	±5	–	–
11	75	±10	78	±10	110	±10	3/(0–20)	32/(0–40)
12	72	±10	71	±10	75	±10	1/(0–20)	4/(0–20)
13	98	±5	68	±10	70	±10	30 (10–40)	0/(0–20)
14	125	±15	65	±5	60	±20	60/(50–70)	5/(0–10)
15	105	±10	160	±10	160	±20	55/(40–60)	0/(0–10)

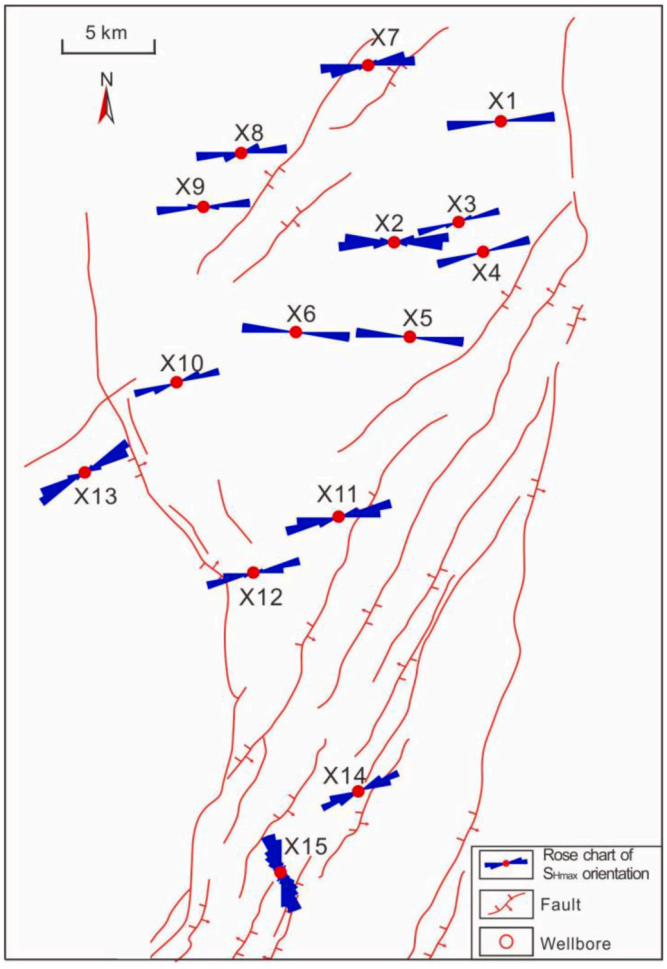

Fig. 6. The orientations of the maximum horizontal stress in the Wufeng-Longmaxi Formations in the Jiaoshiba Area. X7 and X8 wells in the Second and Third Members of the Longmaxi Formation, the other wells in the Wufeng Formation and the First Member of the Longmaxi Formation.

are weakness planes, which could affect the mechanical properties of the rocks (Faulkner et al., 2006) and result in the deflection of the S_{Hmax} orientation (Fig. 5b).

The young's modulus of the underlying Jiancaogou Formation and the Baota Formation limestone is 1.73 times that of the Wufeng-Longmaxi Formation shale. The deviations in the S_{Hmax} orientation caused by the differences in the mechanical properties of these rocks range from 30° to 80° in the Wujiang faulted anticline and the Shimen faulted anticline. However, the variations in the S_{Hmax} orientation in the Jiaoshiba anticline and the Jiangdong slope are less than 30° for the same difference in the mechanical properties of the rocks. Based on the comparison of the geological characteristics of the Jiaoshiba anticline and the Shimen faulted anticline, we concluded that the stress deviations are also influenced by the structural strength. In the structurally stable area, such as the Jiaoshiba anticline, the variations in the S_{Hmax} orientation caused by the differences in the mechanical properties of the rocks are not significant.

5.2. *Effects of fault on the orientation of S_{Hmax}*

Previous studies have reported that the influence of faults on the S_{Hmax} orientation is complex (Sbar et al., 1979; Zoback and Roller, 1979; Zoback et al., 1980; Aleksandrowski et al., 1992; Obara, 1995). The orientation of the S_{Hmax} near a fault can be significantly different from that of the regional stress. In this study, the effects of the mechanical properties and azimuth of the fault on the S_{Hmax} orientation were analyzed based on 17 sets of two-dimensional finite element simulations. The simulation results show that the variation in the S_{Hmax} orientation at the end of a fault is higher than that in the middle of a fault. This is primarily because the tip of the fault is likely to cause stress concentration, which can induce a complicated stress rotation (Okubo and Schultz, 2006). Moreover, these variations increase as the ratio of the Young's modulus of the fault zone (E_1) to that of the surrounding shale (E_2) decreases (Fig. 8a). This means that a broken fault zone could cause large differences between the mechanical properties of the rocks inside and outside of the fault zone, and stress rotation is more likely to occur during tectonic compression. In addition, the influence of the fault on the S_{Hmax} orientation is also affected by the angle (θ) between the fault's strike and the regional stress direction under the same boundary conditions. When the angle (θ) is less than 45°, the variation in the S_{Hmax} orientation exhibits a positive correlation with θ. When the angle (θ) is greater than 45°, the correlation is negative (Fig. 8b).

The shale of the Wufeng-Long 1 Member is widely distributed, and there is little difference in its mechanical properties laterally (Fig. 7). Therefore, contrast in the mechanical properties of the rocks cannot account for the rotation of the S_{Hmax} orientation in the study area. The stress deviations were mainly controlled by the NE-trending and nearly NS-trending faults under the near EW-trending (83°) regional compressive stress. The orientation of the maximum horizontal stress in the middle of fault tends to be consistent with the fault's strike, while the

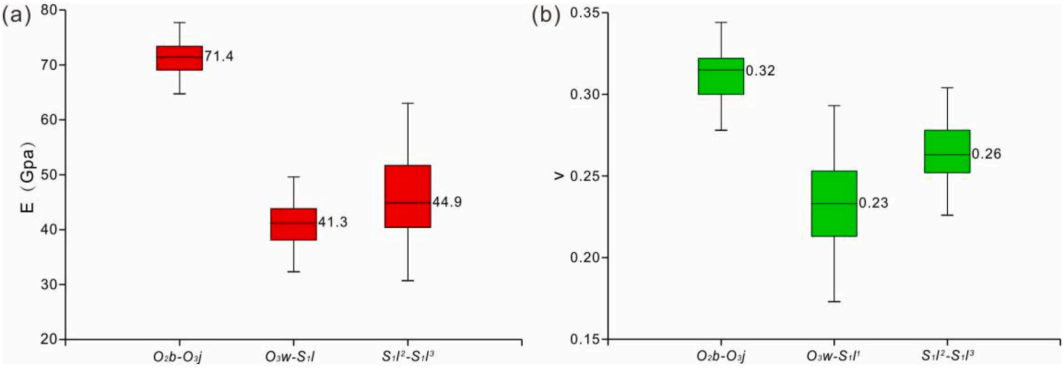

Fig. 7. Rock mechanical properties of different layers in the Jiaoshiba Area (a) Young's modulus (b) Poisson's ratio.

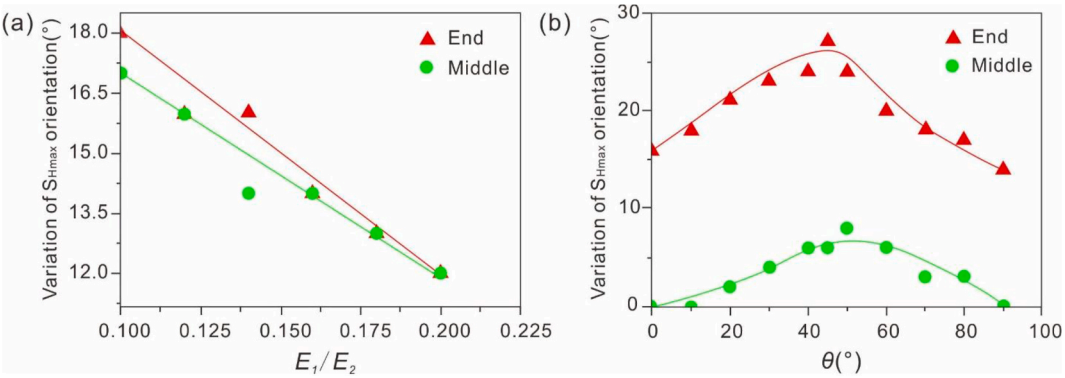

Fig. 8. The variation of maximum horizontal stress orientation near fault. (a) Orientation vibration of S_{Hmax} with the ration of elastic modulus of the fault zone to surrounding shale. (b) Orientation vibration of S_{Hmax} with the angle between the fault orientation and the regional stress orientation (θ).

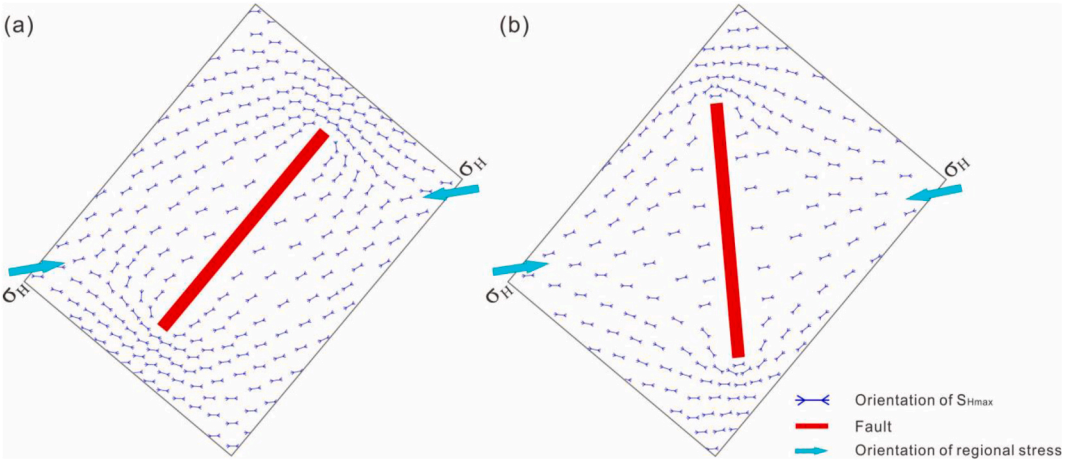

Fig. 9. Orientation of maximum horizontal stress near fault. (a) NE-trending Fault. (b) Nearly NS-trending Fault.

orientation of the S_{Hmax} at the end of the fault tends to be perpendicular to the fault's strike, and the deflection is obviously greater than that in the middle of the fault (e.g., well X15) (Fig. 9). In the study area, the stress variation caused by the mechanical properties of the fault zone ranges from 12° to 18° (Fig. 8a). The angle between the NE fault and the regional stress orientation is 35°–45°, and according to the simulation results, the NE fault could induce the S_{Hmax} orientation to deviate by 6°–28° (Fig. 8b). While the angle between the nearly NS-trending fault and the regional stress direction is 80°–90°, which caused the variation in the stress direction near the fault of 0°–18° (Fig. 8b). Considering the influences of the mechanical properties and the strike of the fault on the maximum horizontal stress orientation, we conclude that the variation in the S_{Hmax} ranges from 18° to 46° due to the influence of the NE-trending faults, while the variation in the S_{Hmax} near the NS-trending faults is 12–36°. The main body of the Jiaoshiba anticline is structurally stable, so there is little variation in the S_{Hmax} orientation. Whereas, the deformation of the southward structure is gradually strengthened, and a NE-trending fault is developed. The orientation of the S_{Hmax} is deflected northward by the influence of the NE-trending fault (Fig. 6). Therefore, the NE-trending fault is the main reason for the lateral deflection of the stress orientation in the Jiaoshiba Area.

6. Conclusions

In this study, the orientation of the maximum horizontal stress in the Jiaoshiba Area of the southeastern Sichuan Basin was inferred from drilling induced fractures observed in resistivity image logs for 15 wells. The stress indicators show that the S_{Hmax} orientation ranges from nearly EW to NEE-SWW in the Jiaoshiba Area. The orientation of the S_{Hmax} exhibits various tendencies both laterally and with burial depth.

The vertical variation in the in-situ stress orientation is controlled by the structural strength and the mechanical properties of the rocks. In the area that has experienced intense tectonic movements, the deviations of the S_{Hmax}, which were caused by the differences in the mechanical properties of the rocks, range from 30° to 80°; while these deviations are usually less than 10° in the area that has experienced weak tectonic movements.

The finite element simulations indicate that the lateral variations in the S_{Hmax} orientations were controlled by the faults, including the different parts of the fault, the mechanical properties of the fault zone, and the fault's strike. The stress rotation near the end of a fault is 14°–21° higher than that in the middle of a fault. Furthermore, the stress variation caused by the mechanical properties of the fault zone ranges from 12° to 18°, and this deviation increases as the Young's modulus of the fault zone decreases. In the study area, the azimuth deflection (18°–46°) of the S_{Hmax} orientation caused by the NE-trending faults is greater than that (12°–36°) caused by the nearly NS-trending faults, which is the main reason for the lateral stress rotation.

Credit author statement

He Tian contributed to FE simulation analyses, DIFs interpretation and wrote the manuscript; Lianbo Zeng provided the idea of the method and outline of the manuscript; Xiang Xu contributed to imaging logs analyses and ideas of this manuscript; Hong Li contributed to data analyses and editing of this manuscript; Bing Luo contributed to ideas, wrote the manuscript and checked the results; Shaoqun Dong contributed to ideas and checked the results.

Declaration of competing interest

The authors declare that they have no known competing financial interests or personal relationships that could have appeared to influence the work reported in this paper.

Acknowledgments

This study was financially supported by the National Natural Science Foundation of China (Grant No.U1663203). The Fundamental Research Funds for the Central Universities (Grant No. 2462020YJRC005).

We thank LetPub (www.letpub.com) for its linguistic assistance during the preparation of this manuscript.

Appendix A. Supplementary data

Supplementary data to this article can be found online at https://doi.org/10.1016/j.jngse.2021.104110.

References

Aadnoy, B.S., Bell, J.S., 1998. Classification of drilling induced fractures and their relationship to in situ stress directions. Log. Anal. 39, 27–42.
Aleksandrowski, P.E., Inderhaug, O.H.E., Knapstad, B.E., 1992. Tectonic structures and wellbore breakout orientation. In: In: the 33th US Symposium on Rock Mechanics (USRMS). American Rock Mechanics Association, pp. 29–37.
Alt, R.C., Zoback, M.D., 2016. In situ stress and active faulting in Oklahoma. Bull. Seismol. Soc. Am. 107 (1), 216–228.
Ameen, M.S., 2014. Fracture and in-situ stress patterns and impact on performance in the Khuff structural prospects, eastern offshore Saudi Arabia. Mar. Petrol. Geol. 50, 166–184.
Barton, C.A., Zoback, M.D., Moos, D., 1995. Fluid flow along potentially active faults in crystalline rock. Geology 23 (8), 683–686.
Barton, C.A., Zoback, M.D., 2002. Discrimination of natural fractures from drilling-induced wellbore failures in wellbore image data-Implications for reservoir permeability: society of Petroleum Engineering Reservoir Evaluation and Engineering. SPE 5 (3), 249–254.
Barton, C., Moos, D., Tezuka, K., 2009. Geomechanical wellbore imaging: implications for reservoir fracture permeability. AAPG Bull. 93 (11), 1551–1569.
Barton, C., Moos, D., 2010. Geomechanical wellbore imaging: key to managing the asset life cycle. In: Peoppelreiter, M., Garcia-Carballido, C., Kraaijveld, M. (Eds.), Diameter and Borehole Image Log Technology. American Association of Petroleum Geologists Memoir, pp. 81–112.
Barba, S., Carafa, M.M.C., Mariucci, M.T., 2010. Present-day stress-field modelling of southern Italy constrained by stress and GPS data. Tectonophysics 482, 193–204.
Bell, J.S., Gough, D.I., 1979. Northeast-southwest compressive stress in Alberta evidence from oil wells. Earth Planet Sci. Lett. 45, 475–482.
Bell, J.S., 1996a. Petro Geoscience 1. In situ stresses in sedimentary rocks (part 1): measurement techniques. Geosci. Can. 23, 85–100.
Bell, J.S., 1996b. Petro Geoscience 2. In situ stresses in sedimentary rocks (part 2): applications of stress measurements. Geosci. Can. 23, 135–153.
Bisdom, K., Bertotti, G., Nick, H.M., 2016. The impact of in-situ stress and outcrop-based fracture geometry on hydraulic aperture and upscaled permeability in fractured reservoirs. Tectonophysics 690, 63–75.
Brudy, M., Zoback, M.D., 1999. Drilling-induced tensile wall fractures: implications for determination of in-situ stress orientation and magnitude. Int. J. Rock Mech. Min. Sci. 36, 191–215.
Brooke-Barnett, S., Flottmann, T., Paul, P.K., Busetti, S., Hennings, P., Reid, R., Rosenbaum, G., 2015. Influence of basement structures on in situ stresses over the Surat Basin, southeast Queensland. J. Geophys. Res.: Solid Earth. 120, 4946–4965.
Cuss, R.J., Rutter, E.H., Holloway, R.F., 2003. Experimental observations of the mechanics of borehole failure in porous sandstone. Int. J. Rock Mech. Min. Sci. 40, 747–761.
Ding, W.L., Fan, T.L., Yu, B.S., Huang, X.B., Liu, C., 2012. Ordovician carbonate reservoir fracture characteristics and fracture distribution forecasting in the Tazhong area of Tarim Basin, Northwest China. J. Petrol. Sci. Eng. 86–87, 62–70.
Faulkner, D.R., Mitchell, T.M., Healy, D., Heap, J., 2006. Slip on 'weak' faults by the rotation of regional stressin the fracture damage zone. Nature 444 (14), 922–925.
Finkbeiner, T., Barton, C.A., Zoback, M.D., 1997. Relationships among in-situ stress, fractures and faults, and fluid flow: monterey formation, Santa Maria Basin, California. AAPG Bull. 81, 1975–1999.
Gale, J.F.W., Reed, R.M., Holder, J., 2007. Natural fractures in the Barnett Shale and their importance for hydraulic fracture treatments. AAPG Bull. 91 (4), 603–622.
Gao, J., He, S., Zhao, J., et al., 2017. Geothermometry and geobarometry of overpressured lower Paleozoic gas shales in the Jiaoshiba field, Central China: insight from fluid inclusions in fracture cements. Mar. Petrol. Geol. 83, 124–139.
Goodman, H.E., Connolly, P., 2007. Reconciling subsurface uncertainty with the appropriate well design using the mechanical Earth model (MEM) approach. Lead. Edge 26, 585–588.
Guo, T., 2013. Evaluation of highly thermally mature shale-gas reservoirs in complex structural parts of the Sichuan Basin (in Chinese with English abstract). J. Earth Sci. 24, 863–873.
Guo, T., Zhang, H., 2014. Formation and enrichment mode of Jiaoshiba shale gas field, Sichuan Basin (in Chinese with English abstract). Petrol. Explor. Dev. 41, 31–40.
Guo, X., Hu, D., Li, Y., Wei, X., Wang, Q., Zhang, H., 2016. Technologies in discovery and exploration of fuling shale gas field, China (in Chinese with English abstract). Nat. Resour. 7, 271–286.
Guo, X.S., 2017. Sequence stratigraphy and evolution model of the wufeng-Longmaxi shale in the upper yangtze area (in Chinese with English abstract). Earth sci. Nat. Gas. Ind. 42 (7), 1069–1081.
He, X.P., He, G.S., Gao, Y.Q., et al., 2018. Geological characteristics and enrichment laws of normal-pressure shale gas in the basin-margin transition zone of SE Chongqing (in Chinese with English abstract), 38 (12), 1–14.
Heidbach, O., Rajabi, M., Reiter, K., Ziegler, M., 2016. World Stress Map 2016. GFZ Data Services.
Higgins, S.M., Goodwin, S.A., Donald, A., Bratton, T., Tracy, G., 2008. Anisotropic Stress Models Improve Completion Design in the Baxter Shale. SPE, Denver, Colorado, pp. 1–10.
Hu, D., Zhang, H., Ni, K., et al., 2014. Main controlling factors for gas preservation conditions of marine shales in southeastern margins of the Sichuan Basin (in Chinese with English abstract). Nat. Gas. Ind. 34 (6), 17–23.
Hu, Z.Q., Zhu, G., Zhang, B.L., Chen, Y., Wei, X., Zhang, L., 2010. Tectonic stress field evolution in fold belts in the northern Upper Yangtze region (in Chinese with English abstract). Chi. J. Geol. 45 (2), 361–379.
Jiu, K., Ding, W.L., Huang, W.H., You, S.G., Zhang, Y.Q., Zeng, W.T., 2013. Simulation of paleotectonic stress field within Paleogene shale reservoirs and prediction of favorable zones for fracture development within the Zhanhua Depression, Bohai Bay Basin, east China. J. Petrol. Sci. Eng. 110, 119–131.
Jones, R.M., Hillis, R.R., 2003. An integrated, quantitative approach to assessing fault-seal risk. AAPG Bull. 347, 189–215.
Ju, W., Sun, W.F., 2016. Tectonic fractures in the lower Cretaceous Xiagou Formation of Qingxi Oilfield, Jiuxi basin, NW China. Part two: numerical simulation of tectonic stress field and prediction of tectonic fractures. J. Petrol. Sci. Eng. 146, 626–636.
Ju, W., Wu, C.F., Wang, K., Sun, W.F., Li, C., Chang, X.X., 2017. Prediction of tectonic fractures in low permeability sandstone reservoirs: a case study of the Es3 m reservoir in the Block Shishen 100 and adjacent regions, Dongying Depression. J. Petrol. Sci. Eng. 156, 884–895.

Ju, W., Li, Z.L., Sun, W.F., Xu, H.R., 2018. In-situ stress orientations in the Xiagou tight oil reservoir of Qingxi Oilfield, Jiuxi Basin, northwestern China. Mar. Petrol. Geol. 98, 258–269.
Ju, W., Wang, K., 2018. A preliminary study of the present-day in-situ stress state in the Ahe tight gas reservoir, Dibei Gasfield, Kuqa Depression. Mar. Petrol. Geol. 96, 154–165.
Kaiser, A., Reicherter, K., Hübscher, C., 2005. Variation of the present-day stress field within the North German Basin—insights from thin shell FE modeling based on residual GPS velocities. Tectonophysics 397 (1–2), 55–72.
Karatela, E., Taheri, A., Xu, C., Stevenson, G., 2016. Study on effect of in-situ stress ratio and discontinuities orientation on borehole stability in heavily fractured rocks using discrete element method. J. Petrol. Sci. Eng. 139, 94–103.
King, R.C., Hillis, R.R., Reynolds, S.D., 2008. In situ stresses and natural fractures in zoothe Northern Perth Basin, Australia. Aust. J. Earth Sci. 55, 685–701.
Ma, Y., Pan, Z., Zhong, N., et al., 2016. Experimental study of anisotropic gas permeability and its relationship with fracture structure of Longmaxi Shales, Sichuan Basin, China. J. Fuel 180, 106–115.
Mohammadnejad, T., Andrade, J.E., 2016. Numerical modeling of hydraulic fracture propagation, closure and reopening using XFEM with application to in-situ stress estimation. Int. J. Numer. Anal. Methods GeoMech. 40 (15), 2033–2060.
Nasehi, M.J., Mortazavi, A., 2013. Effects of in-situ stress regime and intact rock strength parameters on the hydraulic fracturing. J. Petrol. Sci. Eng. 108, 211–221.
Obara, Y., Jang, H., Sugawara, K., 1995. Measurement of stress distribution around fault and considerations. Proc. 2nd Int. Conf. On the Mechanics of Jointed and Faulted Rock, pp. 495–500. Vienna, Balkema, Rotterdam.
Okubo, C.H., Schultz, R.A., 2006. Near-tip stress rotation and the development of deformation band stepover geometries in mode II. GSA Bull 118, 343–348.
Pes˙ka, P., Zoback, M.D., 1995. Compressive and tensile failure of inclined well bores and determination of in situ stress and rock strength. J. Geophys. Res. 100, 12791–12811.
Rajabi, M., Tingay, M., Heidbach, O., 2016. The present-day state of tectonic stress in the Darling Basin, Australia: implications for exploration and production. Mar. Petrol. Geol. 77, 776–790.
Rajabi, M., Tingay, M., King, R., Heidbach, O., 2017. Present-day stress orientation in the Clarence-Moreton Basin of New South Wales, Australia: a new high density dataset reveals local stress rotations. Basin Res. 29, 622–640.
Sbar, M.L., Engelder, T., Plumb, R., 1979. Stress pattern near the San Andreas Fault, Palmdale, California, from near-surface in situ measurements. J. Geophys. Res. Solid Earth 84 (B1), 156–164.
She, X., Chen, J., Zhang, S., Shu, Z.G., Yu, F., Li, D.D., Gong, X.X., 2016. Tectonic characteristics and their shale gas geological significance of the Mesozoic-Paleozoic in Jiaoshiba Area, the Sichuan Basin (in Chinese with English abstract). Oil Gas Geol. 37 (6), 828–837.
Shen, H.C., Cheng, Y.F., Wang, J.Y., 2007. Study of finite element on effects of faults on ground stress field (in Chinese with English abstract). Pet. Geol. Oilfield Dev. Daqing 26 (2), 34–37.
Sibson, R.H., 1996. Structural permeability of fluid-driven fault-fracture meshes. J. Struct. Geol. 18, 1031–1042.
Shu, Y., Lu, Y.C., Bao, H.Y., 2018. Three typical types of shale gas preservation in the fuling shale gas field, Sichuan Basin (in Chinese with English abstract). Nat. Gas. Ind. 38, 31–40, 03.
Tian, H., Zeng, L.b., Shu, Z.G., Bao, H., Xu, X., Mao, Z., Wang, X.Y., 2019. Method for determining elastic parameters for the prediction model of shale transversely isotropic geostress(in Chinese with English abstract). J. Geomech. 25 (2), 166–176.
Tian, H., Zeng, L.B., Xu, X., Shu, Z.G., Peng, Y.M., Mao, Z., Luo, B., 2020. Characteristics of natural fractures of marine shale and their influence on shale gas in Fuling area, Sichuan Basin (in Chinese with English abstract). Oil Gas Geol. 42 (3), 474–483.
Tingay, M., Müller, B., Reinecker, J., Heidbach, O., Wenzel, F., Fleckenstein, P., 2005. Understanding tectonic stress in the oil patch: the World stress map Project. Lead. Edge 24, 1276–1282.
Tingay, M., Morley, C.K., Hills, R.R., Meyer, J., 2010. Present-day stress orientation in Thailand's basins. J. Struct. Geol. 32, 235–248.
Wei, X.F., Guo, T.L., Liu, R.B., 2016. Geochemical features and genesis of shale gas in the Jiaoshiba block shale of fuling shale gas field, chongqing, China (in Chinese with English abstract). J. Nat. Gas Geosci. 361–371.
Wu, L.Y., Lu, Y.C., Jiang, S., 2019. Relationship between the organic-rich shale and geological events of the upper ordovician-lower silurian in the upper yangtza area. Mar. Petrol. Geol. 102, 74–85.
Xu, X., Zeng, L.B., He, T., Ling, K.G., Che, S.Q., Yu, X., Shu, Z.G., Dong, S.Q., 2021. Controlling factors of lamellation fractures in marine shales: a case study of the Fuling Area in Eastern Sichuan Basin, China. J. Petrol. Sci. Eng. 207, 109091.
Yi, X.S., 2017. Sequence Stratigraphy and evolution model of the Wufeng-Longmaxi shale in the upper yangtze area. Earth Sci. 7, 30–43.
Zangeneh, N., Eberhardt, E., Bustin, R.M., 2014. Investigation of the influence of natural fractures and in situ stress on hydraulic fracture propagation using a distinct-element approach. Can. Geotech. J. 52 (7), 926–946.
Zeng, L.B., Li, X.Y., 2009. Fractures in sandstone reservoirs of ultra-low permeability: the upper triassic yanchang Formation in the Ordos basin, China. AAPG Bull. 93 (4), 461–477.
Zeng, L.B., Lyu, W.Y., Li, J., Guo, Y.C., Yang, Y., Dong, S.Q., Liu, X.Z., Zu, K.W., 2019. Variation in the orientation of the maximum horizontal stress in thick channel-fill sandstones with low-permeability: a case of the Bonan Oilfield in the Bohai Bay Basin, eastern China. Mar. Petrol. Geol. 107, 32–40.
Zeng, W.T., Ding, W.L., Zhang, J.C., Zhang, Y.Q., Guo, L., Jiu, K., Li, Y.F., 2013. Fracture development in Paleozoic shale of Chongqing area (South China).Part two: Numerical simulation of tectonic stress field and prediction of fractures distribution. J. Asian Earth Sci. 75, 267e279.
Zoback, M.D., Roller, J.C., 1979. Magnitude of shear stress on the San Andreas fault: implications of a stress measurement profile at shallow depth. Science 206 (4417), 445–447.
Zoback, M.D., Tsukahara, H., Hickman, S., 1980. Stress measurements at depth in the vicinity of the San Andreas fault: implications for the magnitude of shear stress at depth. J. Geophys. Res. Solid Earth 85 (B11), 6157–6173.
Zoback, M.D., Barton, C.A., Brudy, M., Castillo, D.A., Finkbeiner, T., Grollimund, B.R., Moos, D.B., Peska, P., Ward, C.D., Wiprut, D.J., 2003. Determination of stress orientation and magnitude in deep wells. Int. J. Rock Mech. Min. Sci. 40, 1049–1076.
Zoback, M.D., 2007. Reservoir Geomechanics. Stanford University, California, p. 464.